In-plane magnetic anisotropy in strontium iridate Sr_2IrO_4

Muhammad Nauman,[1] Yunjeong Hong,[1] Tayyaba Hussain,[1] M. S. Seo,[2] S. Y. Park,[2] N. Lee,[3] Y. J. Choi,[3] Woun Kang,[4] and Younjung Jo[1,*]

[1]*Department of Physics, Kyungpook National University, Daegu 41566, Korea*
[2]*Spin Engineering Physics Team, Korea Basic Science Institute, Daejeon 34141, Korea*
[3]*Department of Physics, Yonsei University, Seoul 03722, Korea*
[4]*Department of Physics, Ewha Womans University, Seoul 03760, Korea*

(Received 21 July 2017; revised manuscript received 18 September 2017; published 2 October 2017)

Magnetic anisotropy in strontium iridate (Sr_2IrO_4) is found to be large because of the strong spin-orbit interactions. In our work, we studied the in-plane magnetic anisotropy of Sr_2IrO_4 and traced the anisotropic exchange interactions between the isospins in the crystal. The magnetic-field–dependent torque $\tau(H)$ showed a prominent transition from the canted antiferromagnetic state to the weak ferromagnetic (WFM) state. A comprehensive analysis was conducted to examine the isotropic and anisotropic regimes and probe the easy magnetization axis along the *ab* plane. The angle-dependent torque $\tau(\theta)$ revealed a deviation from the sinusoidal behavior, and small differences in hysteresis were observed around 0° and 90° in the low-magnetic-field regime. This indicates that the orientation of the easy axis of the FM component is along the *b* axis, where the antiferromagnetic to WFM spin-flop transition occurs. We compared the coefficients of the magnetic susceptibility tensors and captured the anisotropy of the material. The in-plane $\tau(\theta)$ revealed a tendency toward isotropic behavior for fields with values above the field value of the WFM transition.

DOI: 10.1103/PhysRevB.96.155102

I. INTRODUCTION

Magnetic anisotropic interactions and magnetic anisotropy energy are very useful tools in many industrial and technical fields, ranging from information processing, power distribution and generation, and communication devices, to information storage devices [1–4]. Magnetic anisotropy determines the magnetization stability of a material, whereas the anisotropy energy describes the magnetization tendency of a material along a particular crystallographic direction. The magnetic anisotropic interactions and the associated anisotropic energies have a definite dependence on the crystal symmetry and composition. The exchange interactions between electron spins are completely isotropic, but the orbital magnetization through spin-orbit interactions links the spin magnetization and the atomic structure and induces the magnetic anisotropy in the material [5–7]. Unlike 3*d* transition metal oxides (TMOs) in which the quenching of the orbital angular momentum does not affect the magnetism significantly, 5*d* TMOs are fascinating materials that provide novel electronic states based on strong spin-orbit interactions [8–10]. The interplay of relativistic spin-orbit coupling, Hubbard interaction U, and electronic bandwidth W make the 5d TMOs the best candidates for research in the field of Mott insulators, Weyl semimetals with Fermi arcs, high-temperature superconductivity, correlated topological insulators, Kitaev spin liquids, etc. The higher magnetic anisotropy in 5*d* TMOs is caused by strong spin-orbit interactions [11–17].

Strontium iridate (Sr_2IrO_4) is known as a $J_{\text{eff}} = 1/2$ Mott insulator, in which the strong spin-orbit coupling by Ir ions splits the t_{2g} state into a narrow half-filled $J_{\text{eff}} = 1/2$ state and a wide completely filled $J_{\text{eff}} = 3/2$ state [18–21]. The staggered rotation of the IrO_6 octahedra around the *c* axis at an angle of approximately 11° leads to a distorted Ir–O–Ir in-plane bond angle. Small changes in this canting angle can induce comprehensive changes in the physical properties, and can be achieved by doping or by the application of electric and magnetic fields [8–10]. Below the Curie temperature $T_N \approx 240$ K, the $J_{\text{eff}} = \frac{1}{2}$ isospins of Sr_2IrO_4 display a canted antiferromagnetic (CAF) configuration along the *ab* plane. Thus, the resulting net magnetic moment in each IrO_2 layer is stacked in an up-up-down-down arrangement along the *c* axis. Applying a magnetic field above the critical strength in the *ab* plane generates a single weak ferromagnetic (WFM) state, aligning the net magnetic moment with the field direction. The alignment of the CAF spin moments, coupled with the lattice in Sr_2IrO_4, induces magnetic anisotropy even under very low magnetic fields. The anisotropy of this compound plays a vital role in understanding the underlying phenomena, particularly, those related to the strong spin-orbit coupling, and it can be traced using the anisotropic exchange interactions between the spins in the crystal. There have been nearly no reports on the control of the t_{2g} orbital states, through externally applied magnetic fields, because of the antiferromagnetic (AFM) configurations in such systems, which are very rarely sensitive to the applied magnetic field. However, the canting along the in-plane direction in Sr_2IrO_4 makes an interesting playground to study the responses to the changing magnitudes and directions of the applied magnetic field.

A previous report on the out-of-plane torque measurements in the Sr_2IrO_4 crystal showed that the WFM component along the in-plane direction was stimulated by the in-plane component of the magnetic field alone, and that the *c* axis was a hard axis [22]. The Raman scattering study was performed to examine the magnetic-field–dependent spin dynamics of Sr_2IrO_4. Valuable anisotropic effects were demonstrated along the in-plane direction, in the presence of an external magnetic

*jophy@knu.ac.kr

field below 1.5 T, and isotropic spin dynamics were observed above 1.5 T. Longitudinal and transverse magnetization measurements considering the in-plane magnetic anisotropy using torque magnetometry revealed fourfold periodicity in Sr_2IrO_4. A change from the metastable to a nearly sinusoidal behavior, above a magnetic field of 0.1 T, was also reported [23].

In our study, we performed in-plane magnetic anisotropy measurements of Sr_2IrO_4 single crystals in the low-magnetic-field regions. The nature of the alignment of the magnetic moments and the spin-flop transitions under the applied magnetic fields were studied using torque magnetometry. The nature of the arrangement of the magnetic moments could be determined by performing angle-dependent torque measurements $\tau(\theta)$ in the basal plane. This provided a method to study the contribution of in-plane anisotropy to the total magnetic anisotropy of the system, the shape anisotropy being almost negligible in the current case. The $\tau(\theta)$ for low magnetic fields deviated from the sinusoidal behavior, and small differences in hysteresis existed around 0° and 90°. The difference between the a and b axes along the in-plane was confirmed by comparing the coefficients of susceptibility tensors. We concluded that the magnetic anisotropy exists under a small magnetic field and that Sr_2IrO_4 tends to be isotropic above the WFM transition field. The b axis was found to be an easy axis of magnetization along the ab plane.

II. EXPERIMENTAL DETAILS

Sr_2IrO_4 crystals were prepared by a flux method using $SrCl_2$ as flux. Crystallinity was confirmed by x-ray diffraction studies. The Sr_2IrO_4 single crystal was mounted on a piezoresistive cantilever and the change in the torque was measured from the change in the resistance of the piezomaterial constituting a Wheatstone bridge circuit. The crystal axes of the a and b directions are shown in Fig. 1(a). As the crystal was too small to determine the crystal axis properly in the plane, one edge was defined as the a axis and the vertical direction was defined as the b axis. We evaluated the magnetic anisotropy in terms of the components of the magnetic susceptibility tensor $\vec{M}$ for fields $\vec{H}$ applied along different crystallographic directions, i.e., $\vec{\tau_c} = \vec{M} \times \vec{H}$. The direction of the magnetic field applied to the sample was controlled by a resistive magnet and rotator. We measured the magnetic-field–dependent torque $\tau(H)$ and the angle-dependent torque $\tau(\theta)$ of Sr_2IrO_4; the angle θ is the direction of the applied field with respect to the a axis shown in Fig. 1(b).

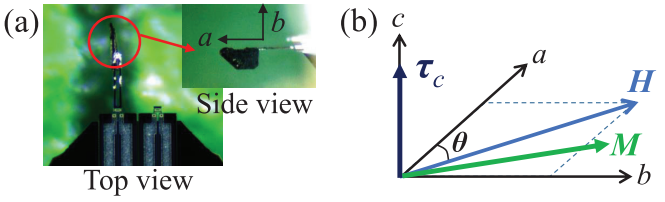

FIG. 1. (a) Orientation of the crystal mounted on a piezoresistive cantilever. (b) Sketch of the in-plane rotation for torque measurements. The angle θ is the direction of the field with respect to the a axis.

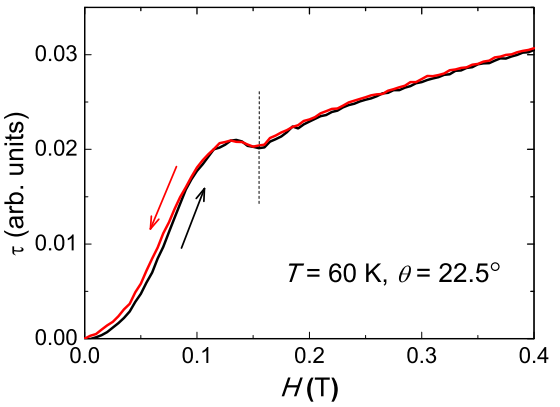

FIG. 2. Field-dependent torque measurement at $T = 60$ K and $\theta = 22.5°$. A small kink around 0.15 T indicates a weak ferromagnetic transition.

III. RESULTS AND DISCUSSION

Figure 2 shows the $\tau(H)$ resulting from the application of a magnetic field at $T = 60$ K and $\theta = 22.5°$. The field dependence at low magnetic fields is not linear, and it exhibits a steep slope relative to the $\tau(H)$ at high magnetic fields. This represents a rapid change in the antiferromagnetic domain alignment as well as in the vertical component of the antiferromagnetically coupled moment in the presence of an external magnetic field. A small kink appears at 0.15 T, and the WFM spin-flop transition occurs. The saturation of magnetization after the WFM transition field can be considered to lock magnetization in a certain direction, to minimize the total energy of the system. A small hysteretic effect can be traced, which disappears above 0.15 T.

We measured the angle dependence of the torque $\tau(\theta)$ at 60 K under various magnetic fields, and a contour plot is shown in Fig. 3. The background signal at $H = 0$ curve has been subtracted from the $\tau(\theta)$. The sketch on the right-hand

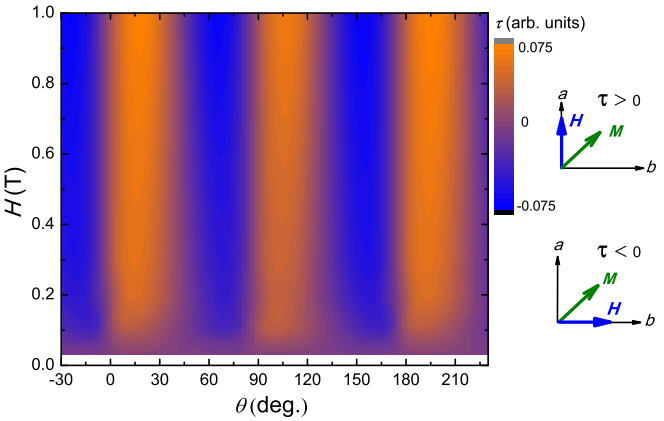

FIG. 3. Contour plot of $\tau(\theta)$ for various magnetic fields. Alternation of negative and positive torque is observed.

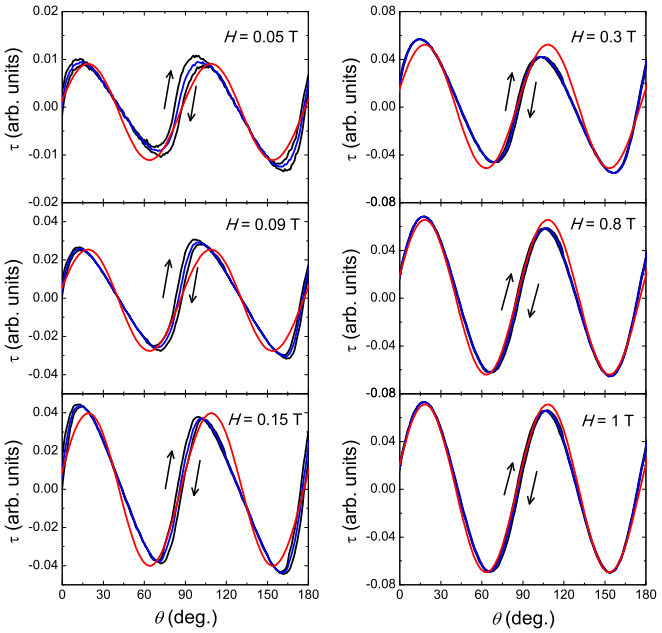

FIG. 4. In-plane angular dependence of torque (black line) under different magnetic fields. The blue line represents the average value of $\tau(\theta)$ between increasing and decreasing angles. The red line is the curve fitted using Eq. (1).

side of Fig. 3 explains the alternation of the negative and positive torque values as the magnetic field rotates along the ab plane. The change in the negative and positive torque values for each 45° angle change can be attributed to the different directions of the net magnetization for each domain, in response to the changing magnetic field. In the case of isotropic antiferromagnets, the magnetic easy axis of spin is aligned perpendicular to the magnetic field. In anisotropic antiferromagnets, the magnetic easy axis is easily reoriented from the direction of the crystal axis, owing to the competition between the Zeeman energy and the anisotropic energy. The new direction of the easy axis is determined by the magnitude and direction of the applied magnetic field [24].

Figure 4 shows the individual $\tau(\theta)$ for several magnetic fields. The lower the temperature is, the smaller the noise effect and the better the signal will be. The $\tau(\theta)$ in the low-field region tends to deviate from the sinusoidal form, owing to the sawtoothlike response of the sample in this field region, whereas the $\tau(\theta)$ in the high-field region represents the sin2θ pattern well, similar to the results reported by L. Frutcher *et al.* [23]. An incomplete 90° symmetry at low fields can be found from the difference in amplitude due to the tilted alignment of the sample, whereas a perfect 90° symmetry can be detected at higher fields. Deviation from the sinusoidal function at low magnetic fields indicates the orientation of the easy axis of the magnetic component, but a sharp change in torque shows the spin-flop AFM to WFM transition. That is, the hysteresis effect indicates an easy magnetization axis and a spin-flop transition near 90°. Reduction in the hysteresis effect at high magnetic fields represents the ordering of the domain magnetization in certain directions and the weakening of magnetic canting. We can recognize a magnetic easy axis in the sin2θ pattern. The

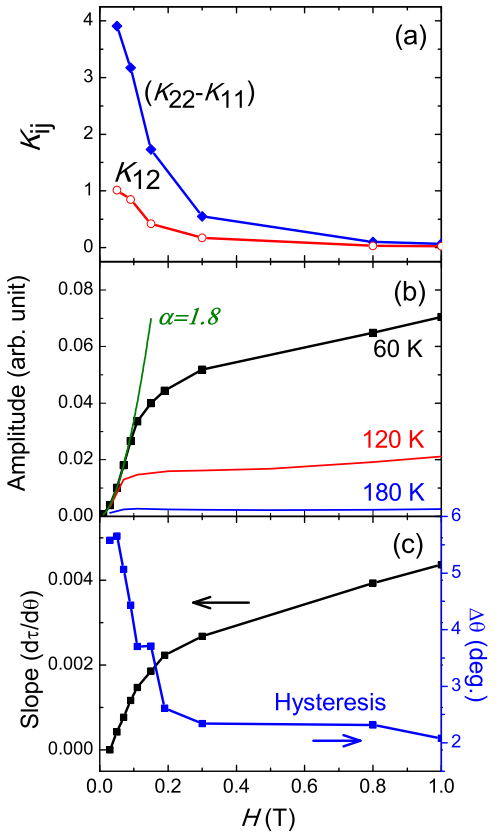

FIG. 5. (a) Coefficient of magnetic susceptibility tensor (K_{ij}) vs. applied magnetic field (H), (b) maximum amplitude $A(H)$ obtained from the fitting of $\tau(\theta)$ at different temperatures, (c) variations in slope changes (dτ/dθ) in the range between 38° and 48° from a linear fit, and hysteresis $\Delta\theta$ with the applied magnetic field.

blue line in Fig. 4 is the average value of $\tau(\theta)$ with increasing and decreasing angles. The red line is the fitting curve obtained using Eq. (1):

$$\tau(\theta) = \frac{\cos\theta}{|\cos\theta|}\frac{B\sin\theta\sin^2\varphi}{\sqrt{1+\tan^2\theta\cos^2\varphi}}H + [(K_{22}-K_{11})\sin2\theta + 2K_{12}\cos2\theta]H^2, \quad (1)$$

where θ is the angle formed by the external magnetic field (H) and the a axis, φ is the tilt angle of the sample, which contributes to the out-of-plane torque, $K_{22}-K_{11}$ is the difference in the coefficients of susceptibility tensors according to the two principal crystallographic directions, and K_{12} is the coefficient of the susceptibility tensor along the ab plane. The first term in Eq. (1) represents the WFM contribution, and the second term represents the AFM contribution. We have found that the WFM term is negligible, and that the AFM contribution dominates the in-plane $\tau(\theta)$ data.

We compare the field dependences of $(K_{22}-K_{11})$ and K_{12} in Fig. 5(a). A positive value obtained for $(K_{22}-K_{11})$ stipulates a larger value for K_{22}. It is noted that $(K_{22}-K_{11})$ is greater than K_{12}, which supports the magnetic in-plane anisotropy in the low-magnetic-field regime. The difference between $(K_{22}-K_{11})$ and K_{12} decreases with the field,

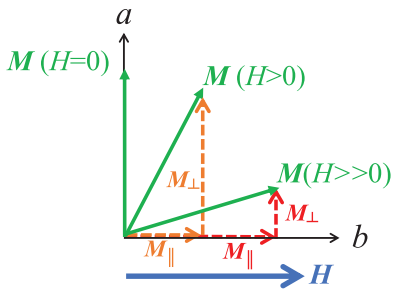

FIG. 6. Sketch of changing domain magnetization (M) with increasing H. The magnetization component along the b axis ($M_{\parallel}$) describes the WFM contribution.

and the system tends toward isotropic behavior. According to the fitting of $\tau(\theta)$, we obtain the maximum amplitude $A(H)$ as shown in Fig. 5(b). $A(H)$ represents the dominant contribution of the CAF magnetic moment, where the WFM component is linear and the AFM component shows a square dependence on the magnetic field. The power law, $A(H) \sim H^{\alpha}$, can be used to assess the degrees of AFM and WFM contributions. Below 0.1 T, the exponent α is between 1.8 and 2.0, indicating the dominance of the AFM contribution. $A(H)$ deviates from $H^{1.8}$, and α decreases with the field. The nearly linear tendency of $A(H)$ above 0.15 T indicates the WFM contribution. The saturation of $A(H)$ indicates that parallel alignment of the induced magnetization field occurs. It does not affect the torque, and the spin axis aligns substantially perpendicular to the magnetic field. Currently, the reason for the deviation of the fitted curve at lower fields is unclear.

One of the main causes of the hysteresis effect is the slow dynamics of the domain wall motion. When the time scale of the domain wall motion is comparable to that of the dynamics of the torque measurement, it results in a hysteresis effect [25]. Another contribution to the hysteresis comes from the equally populated twin domains, where one domain prefers a particular crystallographic orientation. During the in-plane rotation of the magnetic field, the magnetic domains cannot follow the in-plane rotation of the magnetic field because the magnetic field is too small to align and rotate the moments along the field direction. Figure 5(c) shows the exponential decrease in the degree of hysteresis ($\Delta\theta$) with increasing magnetic field. The reduction in the hysteresis effect is rapid up to 0.2 T, whereas it tends to saturate for larger magnetic fields where the AFM and WFM states coexist. A possible analysis of the emergence of hysteresis is based on the AFM twin domains. The Zeeman energy contribution induces the magnetic moment of a twin domain along a specific crystallographic direction while minimizing the total energy of the system. The new orientation of the net magnetic moment depends on the magnitude and direction of the applied magnetic field. In Fig. 5(c), we also plot the slope of $\tau(\theta)$ in the range between 38° and 48°, from a linear fit. It is noted that in-plane anisotropy exists at low magnetic fields, less than 0.2 T. The increase in slope with increasing magnetic field is consistent with the sawtooth motion at low fields and the sinusoidal pattern at high fields.

Figure 6 illustrates the magnetization alignment of each layer as the magnetic field increases along the b axis. The FM component ($M_{\parallel}$) varies with increasing field, although the sample does not change completely from a mixed AFM-WFM to a complete FM phase owing to the canting. However, a nonzero value with a sinusoidal period of $\tau(\theta)$ results from a partially dominant FM component. It was reported that a change of less than 0.1° in the canting angle results in comprehensive changes in properties regarding magnetic ordering [26]. An increase in the magnetization component along the b axis (i.e., $M_{\parallel}$) describes the emergence of a WFM contribution with increasing magnetic field; this supports the steeper slope for the low magnetic field shown in Fig. 2. The perpendicular component of magnetization ($M_{\perp}$) decreases; hence, a smaller slope can be perceived after the transition field, in Fig. 2.

IV. CONCLUSIONS

A distinct magnetic anisotropy exists along the basal plane of Sr_2IrO_4 in low-magnetic-field regions below 0.15 T. The magnetic in-plane anisotropy of Sr_2IrO_4 in the low-magnetic-field regime was observed with torque measurements under a magnetic field along the basal plane. The field-dependent torque measurements showed a pronounced transition from CAF to WFM around 0.15 T. The angle-dependent torque measurements showed a distinct field-squared dependence in low-magnetic-field regions and a dominant emergence of the WFM contribution, above 0.15 T. The significant contribution from AFM behavior at low fields and the emergence of WFM on increasing the magnetic field were confirmed. The sharp decrease in the $\tau(\theta)$ amplitude around 90° for in-plane measurements in the low-magnetic-field regime supported the spin-flop transition in the vicinity of the easy magnetization axis along the in-plane. The coefficients of the magnetic susceptibility tensors confirmed the easy magnetization axis along the ab plane. The reorientation of magnetic moments and their field dependences in both low- and high-magnetic-field regions clearly demonstrated the change in the canting and magnetization components of the sample.

ACKNOWLEDGMENTS

The work at Kyungpook National University was supported by the Brain Korea (BK) and the National Research Funding (NRF) [Grants No. 2013R1A1A2063904 and No. 2016R1A2B4016656] by the Korean Government. The work at Yonsei University was supported by the NRF Grants No. NRF-2014S1A2A2028481, No. NRF-2015R1C1A1A02037744, No. NRF-2016R1C1B2013709, No. NRF-2017K2A9A2A08000278, and No. 2017R1A5A1014862 (SRC program: vdWMRC center) and partially by the Yonsei University Future-leading Research Initiative of 2014 (Grant No. 2016-22-0099). W.K. was supported by an NRF grant funded by the Korea Government (MSIP) (Grant No. 2015-001948). A portion of this work was supported by the National Research Council of Science & Technology (NST) (Grant No. CAP-16-01-KIST) by the Korean government (MSIP).

[1] P. Gambardella, S. Rusponi, M. Veronese, S. Dhesi, C. Grazioli, A. Dallmeyer, I. Cabria, R. Zeller, P. Dederichs, and K. Kern, Science **300**, 1130 (2003).
[2] K. Adachi, T. Suzuki, K. Kato, K. Osaka, M. Takata, and T. Katsufuji, Phys. Rev. Lett. **95**, 197202 (2005).
[3] L. Szunyogh, B. Lazarovits, L. Udvardi, J. Jackson, and U. Nowak, Phys. Rev. B **79**, 020403 (2009).
[4] S. Ouazi, S. Vlaic, S. Rusponi, G. Moulas, P. Buluschek, K. Halleux, S. Bornemann, S. Mankovsky, J. Minár, and J. B. Staunton, Nat. Commun. **3**, 1313 (2012).
[5] M. K. Crawford, M. A. Subramanian, R. L. Harlow, J. A. Fernandez-Baca, Z. R. Wang, and D. C. Johnston, Phys. Rev. B **49**, 9198 (1994).
[6] J. C. Martinez, S. H. Brongersma, A. Koshelev, B. Ivlev, P. H. Kes, R. P. Griessen, D. G. de Groot, Z. Tarnavski, and A. A. Menovsky, Phys. Rev. Lett. **69**, 2276 (1992).
[7] A. Cornia, A. G. M. Jansen, and M. Affronte, Phys. Rev. B **60**, 12177 (1999).
[8] P. Radaelli and S. Dhesi, Philos. Trans. R. Soc. London A **373**, 20130148 (2015).
[9] C. Wang, H. Seinige, G. Cao, J.-S. Zhou, J. B. Goodenough, and M. Tsoi, Phys. Rev. X **4**, 041034 (2014).
[10] B. Kim, H. Ohsumi, T. Komesu, S. Sakai, T. Morita, H. Takagi, and T. Arima, Science **323**, 1329 (2009).
[11] F. Wang and T. Senthil, Phys. Rev. Lett. **106**, 136402 (2011).
[12] G. Jackeli and G. Khaliullin, Phys. Rev. Lett. **102**, 017205 (2009).
[13] B. J. Kim, H. Jin, S. J. Moon, J.-Y. Kim, B.-G. Park, C. S. Leem, J. Yu, T. W. Noh, C. Kim, S.-J. Oh, J.-H. Park, V. Durairaj, G. Cao, and E. Rotenberg, Phys. Rev. Lett. **101**, 076402 (2008).
[14] G. Cao, T. F. Qi, L. Li, J. Terzic, S. J. Yuan, L. E. DeLong, G. Murthy, and R. K. Kaul, Phys. Rev. Lett. **112**, 056402 (2014).
[15] A. A. Burkov and L. Balents, Phys. Rev. Lett. **107**, 127205 (2011).
[16] J. Chaloupka, G. Jackeli, and G. Khaliullin, Phys. Rev. Lett. **105**, 027204 (2010).
[17] X. Wan, A. M. Turner, A. Vishwanath, and S. Y. Savrasov, Phys. Rev. B **83**, 205101 (2011).
[18] L. Miao, H. Xu, and Z. Q. Mao, Phys. Rev. B **89**, 035109 (2014).
[19] O. Krupin, G. Dakovski, B. Kim, J. Kim, J. Kim, S. Mishra, Y.-D. Chuang, C. Serrao, W. Lee, and W. Schlotter, J. Phys.: Condens. Matter **28**, 32LT01 (2016).
[20] M. Miyazaki, R. Kadono, M. Hiraishi, A. Koda, K. M. Kojima, K. Ohashi, T. Takayama, and H. Takagi, Phys. Rev. B **91**, 155113 (2015).
[21] H. Gretarsson, N. H. Sung, M. Höppner, B. J. Kim, B. Keimer, and M. LeTacon, Phys. Rev. Lett. **116**, 136401 (2016).
[22] Y. Hong, Y. Jo, H. Y. Choi, N. Lee, Y. J. Choi, and W. Kang, Phys. Rev. B **93**, 094406 (2016).
[23] L. Fruchter, D. Colson, and V. Brouet, J. Phys.: Condens. Matter **28**, 126003 (2016).
[24] M. Herak, M. Miljak, G. Dhalenne, and A. Revcolevschi, J. Phys.: Condens. Matter **22**, 026006 (2009).
[25] M. Herak, H. Berger, M. Prester, M. Miljak, I. Živković, O. Milat, D. Drobac, S. Popović, and O. Zaharko, J. Phys.: Condens. Matter **17**, 7667 (2005).
[26] M. Ge, S. Tan, Y. Huang, L. Zhang, W. Tong, L. Pi, and Y. Zhang, J. Magn. Magn. Mater. **345**, 13 (2013).